Activation of skeletal muscle-resident glial cells upon nerve injury

Daisy Proietti, Lorenzo Giordani, Marco de Bardi, Chiara d'Ercole, Biliana
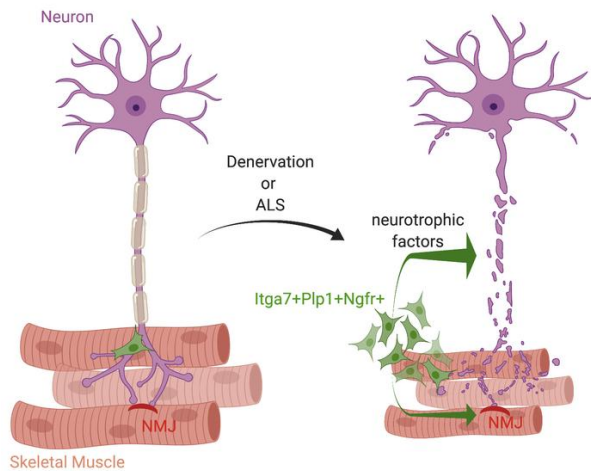Lozanoska-Ochser, Susanna Amadio, Cinzia Volontè, Sara Marinelli, Antoine
Muchir, Marina Bouchè, et al.

Activation of skeletal muscle-resident glial cells upon nerve injury

Daisy Proietti, … , Pier Lorenzo Puri, Luca Madaro

Research In-Press Preview **Muscle biology**

Graphical abstract

1 **TITLE PAGE**

2

3 **Title**

4 Activation of skeletal muscle-resident glial cells upon nerve injury

5

6 **Authors**

7 Daisy Proietti[1,2], Lorenzo Giordani[3], Marco De Bardi[1], Chiara D'Ercole[2], Biliana Lozanoska-

8 Ochser[2], Susanna Amadio[1], Cinzia Volontè[1-4], Sara Marinelli[5], Antoine Muchir[3], Marina Bouchè[2],

9 Giovanna Borsellino[1], Alessandra Sacco[6], Pier Lorenzo Puri[6] and Luca Madaro[1,2,7]*

10

11 **Affiliations**

12 [1] IRCCS Fondazione Santa Lucia (FSL); Rome; Italy

13 [2] Dept AHFMO, University of Rome "la Sapienza", Via A. Scarpa 14, 00161 Rome, Italy

14 [3] Sorbonne Université, INSERM UMRS 974, Association Institut de Myologie, Centre de

15 Recherche en Myologie, 75013 Paris, France.

16 [4] CNR, Institute for Systems Analysis and Computer Science, Via Dei Taurini 19, 00185 Rome

17 [5] CNR - National Research Council, Institute of Biochemistry and Cell Biology, 00015

18 Monterotondo Scalo (RM), Italy.

19 [6] Development, Aging and Regeneration Program, Sanford Burnham Prebys Medical Discovery

20 Institute, La Jolla, CA, USA

21 [7] Lead Contact

22 *Correspondence: Luca Madaro, via Antonio scarpa 14/16 00143 Rome (Italy), +39 0649766573
23 luca.madaro@uniroma1.it

24

25

26 **Conflict of interest statement**

27 The authors have declared that no conflict of interest exists.

28

29 **ABSTRACT**

30 Here, we report on the identification of Itga7-expressing muscle resident glial cells activated by loss

31 of NMJ integrity. Gene expression analysis at bulk and single cell level revealed that these cells are

32 distinct from Itga7-expressing muscle satellite cells. We show that a selective activation and

33 expansion of Itga7-positive glial cells occurs in response to muscle nerve lesion. Upon activation,

34 muscle glial-derived progenies expressed neurotrophic genes, including Ngfr, which enables their

35 isolation by FACS. We show that activated muscle glial cells also expressed genes potentially

36 implicated in ECM remodeling at NMJs. Among them, we observed Tenascin C (Tnc), which was

37 highly expressed by muscle glial cells activated upon nerve injury, and preferentially localized to

38 NMJ. Interestingly, we observed that while the activation of muscle glial cells by acute nerve injury

39 was reversible, upon NMJ repair. By contrast, in a mouse model of Amyotrophic Lateral Sclerosis

40 (ALS), in which NMJ degeneration is progressive, muscle glial cells steadily increased over the

41 course of the disease; however, they exhibited an impaired neurotrophic activity, suggesting that

42 pathogenic activation of glial cells may be implicated in ALS progression.

43

44

INTRODUCTION

Skeletal muscle homeostasis is maintained by a large network of muscle-resident cells, that coordinate the response to homeostatic perturbations, such as muscle or nerve injury (1, 2).

Among these cells, muscle satellite cells (MuSCs) are the bonafide muscle stem cells that exist in a quiescent state during homeostasis in adult tissues and become activated in response to acute muscle damage or in chronic degenerative conditions (3–8). In addition to their absolute requirement for regeneration of injured muscle, recent studies have reported that MuSCs may also participate in the maintenance of neuro-muscular junction (NMJ) integrity and regeneration upon nerve injury (9, 10). Nerve injury and repair are events closely associated with the process of muscle regeneration; however, the precise contribution of MuSCs to NMJ regeneration is poorly understood. Likewise, whether additional muscle-resident cell types contribute to neurite growth and extension toward regenerating fibers to restore functional NMJs remains unknown.

We and others have recently reported on the activation of muscle-resident mesenchymal progenitors – the fibro adipogenic progenitors (FAPs), and their expansion following denervation (11). In addition to FAPs, resident macrophages have also been implicated in the process of NMJ repair following denervation or injury (9, 10, 12, 13). Interestingly, alterations in function and number of MuSCs and FAPs have been observed in neuromuscular disorders, such as Amyotrophic Lateral Sclerosis (ALS), in which loss of NMJ integrity occurs progressively (14, 15)

In postnatal life, the disruption of skeletal muscle-nerve cross talk leads to muscle atrophy and fibrosis (16–18), eventually leading to irreversible paralysis in conditions of complete nerve loss (i.e. traumatic spinal cord injury) or progressive loss of NMJ (e.g. chronic neuromuscular disorders) (19). Therefore, identification of the cell types activated by nerve injury and an improved understanding of their functional interactions is imperative in order to develop novel therapeutic strategies to counter the effect of muscle denervation.

In this study, we performed gene expression analysis in both bulk and single cells isolated from limb muscle following nerve injury with the aim to identify the cellular players that might contribute to nerve repair.

3

RESULTS

Nerve injury activates a neurotrophic program in Itga7+ non-satellite cells

The contribution of Itga7-expressing MuSCs to the maintenance of NMJ integrity, and regeneration upon nerve injury was previously reported by Liu et al 2015 and Liu et al. 2017 (9, 10). These studies prompted our interest in the transcriptional profiles of Itga7+ cells isolated from limb muscles of mice either unperturbed or exposed to nerve injury. To this end, we performed RNAseq analysis on Itga7+/Sca1-/Ln- cells (from now on, referred to as Itga7+ cells) isolated by FACS from limb muscles of 3-month-old mice, at 3 days after denervation by sciatic nerve severing, and compared to Itga7+ cells isolated from control mice. Heatmap comparison revealed extensive alterations of the transcriptional profile in Itga7+ cells isolated post-nerve injury, compared to unperturbed controls, with a clear bias toward up-regulation of genes which accounted for the vast majority of the differentially expressed genes (Figure 1a). Notably, most of the upregulated genes were those associated with neuronal growth and repair pathways, including Nerve Growth Factor Receptor (Ngfr), Sonic Hedgehog (Shh) Tenascin-C (Tnc), Neuronal Cell Adhesion Molecule (NRCAM), Glial Cell Derived Neurotrophic Factor (Gdnf), and the glial lineage-specific transcription factors Oligodendrocyte lineage genes (Olig1) (Figure 1a). Other genes of alternative mesenchymal lineages, but recently implicated in neurogenesis (e.g. Runx2) (20) were also found upregulated in Itga7+ cells isolated following nerve injury. Moreover, gene ontology analyses of RNAseq data predicted the activation of "nervous system development" and "axon guidance" among the main activated pathways (Figure 1b).

The upregulation of neurotrophic genes in Itga7+ cells after denervation suggests that this population includes cell types endowed with potential nerve repair activities. Thus, in order to identify this population, we sought to determine whether the activation of the neurotrophic gene program also occurred in Itga7+ cells isolated from muscles subjected to sciatic nerve crush - a reversible lesion that is typically followed by repair and restoration of NMJ integrity (21). Indeed, the upregulation of neurotrophic genes was also detected by qPCR analysis in Itga7+ cells following sciatic nerve crush (Figure 1c). Interestingly, activation of the same genes was also observed in cells

102   isolated using the Satellite Cells isolation kit (Miltenyi Biotec) magnetic strategy that is based on

103   lineage marker exclusion of Itga7-negative muscle-resident cells (Suppl. Figure 1a).

104   Given the recent studies showing that Itga7-expressing cell populations in muscle include

105   cellular subsets divergent in developmental origin from the actual MuSCs (22), we utilized the

106   PAX7^{CreER};tdTomato$^{f/f}$ mouse model, which allows MuSCs lineage tracing (23), in order to

107   unequivocally determine whether the activation of the neurotrophic gene program occurs in MuSCs

108   or the non-MuSC cell fraction among the Itga7+ cells. In this mouse model, tamoxifen treatment

109   leads to the permanent expression of tomato fluorescent protein in Pax7+ MuSCs (Suppl. Figure

110   1b). Seven days after tamoxifen treatment, 3-month-old mice were subjected to nerve injury and

111   analyzed 3 days later (Figure 1d). As expected, Itga7+Tomato+ cells isolated from limb muscles of

112   uninjured mice or following sciatic nerve crush expressed high level of the MuSC-identity genes

113   Pax7 and Vcam1, whereas the Itga7+Tomato- cell population did not express these markers

114   (Figure1e). However, upon denervation, only the Itga7+Tomato- fraction expressed Ngfr, Shh, Tnc,

115   Nrcam and Gdnf, indicating the induction of a neurotrophic signalling pathway in the Pax7-negative

116   fraction of Itga7+ cells (Figure 1e, Suppl. Figure 1c). These observations also indicate that among

117   the cells isolated with the Satellite Cells isolation kit (Miltenyi Biotec), non-myogenic Itga7+ and Pax7

118   negative cell types might also co-segregate with the myogenic fraction.

119   Overall, these findings show transcriptional activation of a neurotrophic program in the non-

120   myogenic fraction of Itga7+ cells and suggest their potential involvement in the functional cross-talk

121   between muscle resident cells and NMJ in response to nerve injury.

122

123   *scRNA-seq reveals heterogeneity within the Itga7+ muscle resident cells*

124   Recently, the heterogeneous composition of muscle resident mononuclear cells has been

125   dissected using high resolution cartography by scRNA-seq. This strategy has revealed the identity

126   of a new MuSCs-independent myogenic population among the Itga7+ cells, referred to as Smooth

127   Muscle Mesenchymal Cells (SMMCs) (22). To further determine whether the activation of the

128   neurotrophic program upon nerve injury occurred in SMMC or in other sub-populations within Itga7+

129   cells, we performed single-cell RNA-seq (scRNA-seq) transcriptome profiling in Itga7+ cells isolated

from limb muscles of mice 3 days following sciatic nerve crush or control mice. By using the 10x

Genomics' single-cell RNA-seq (scRNA-seq) technology we obtained a total of 3949 cells analyzed.

Clustering analysis identified 11 different groups (Suppl. Figure 2a). Based on markers expression

we could clearly identify three major populations that were composed of multiple sub-clusters (Figure

2a-b). In particular, we detected MuSCs, as Pax7+, Myf5+ and Vcam1+ expressing cells, smooth

muscle mesenchymal cells (SMMCs), as Myh11+ expressing cells and glial cells as Plp1 and Mpz

expressing cells (Figure 2a).

Interestingly, within the SMMCs cell population we could distinguish a Myl9+Rgs5^{low} and

Myl9+Rgs5^{high} subpopulations (Suppl. Figure 2b). In line with this observation, Rgs5, Myl9 and Plp1

expression was evident in the tomato-negative fraction of tamoxifen treated PAX7.Cre_tdTomato

mice (Suppl. Figure 2c). The gene expression profile of the smaller clusters (less than 150 cells) was

indicative of myotendinous (Scx^{high} expressing cells), endothelial (Pecam1^{high}) and mesenchymal (as

Ly6a/Ly6e^{pos} and Pdgfra^{pos}) lineages (Figure 2b). However, it is likely that the presence of these

clusters is due to contamination from Itga7$^{low/neg}$ populations.

Plp1+ glial cells are the major Itga7+ population responsive to denervation.

We focused our analysis on the three major cell types identified by scRNAseq analysis

among the Itga7+ cells isolated following nerve injury – i.e. MuSCs, SMMCs and glial cells. We

observed a similar distribution of MuSCs and SMMCs in both healthy and denervated muscle (Figure

3a). By contrast, we observed a specific increase in Plp1+ cells in response to nerve injury. To

validate this finding, we denervated mice by nerve crush injury, and at 12h before harvest we

administered an intraperitoneal injection of EdU. EdU incorporation analysis revealed a significant

proportion of proliferating Plp1+ cells at 3 days following sciatic nerve crush (Suppl. Figure 3a). The

gene expression profile of nerve injury-activated Plp1+ cells largely overlapped with those of glial

cells recently described by both De Micheli et al. and Giordani et al. (22, 24) (Suppl. Figure 3b);

however, there was no significant overlap with other populations (in particular with MuSCs and

SMMCs) (Suppl. Figure 3b). In addition, these cells were enriched in additional markers known to

be expressed by glial/Schwann cells (Suppl. Figure 3c).

158   Furthermore, we noted extensive alterations in gene expression in Plp1+ cells following nerve

159   injury, compared to control muscle, while only a few genes were significantly altered in MuSCs and

160   SMMCs (Suppl. Figure 3d). Single cell RNAseq analysis revealed that Plp1+ glial cells are

161   characterized by a neurotrophic signature (Figure 3b-c and Suppl. Figure 3d), with most of the

162   upregulated genes coinciding with those identified in the bulk Itga7+ cells shown in Figure 1 – i.e.

163   Ngfr, Tnc, Gdnf, Runx2 and other genes strictly related to nerve development (Figure 3b-c). Among

164   these genes, the Ngfr was used to identify these cells, since it was found to be specifically expressed

165   in glial-cells, and no other muscle resident cells, in response to nerve injury, by an independent

166   scRNAseq analysis post-denervation (25). It is interesting to note that Hicks et al. have previously

167   shown that Ngfr is transiently expressed in human MuSC progenitors during the generation of hiPSC-

168   derived MuSCs (26). Our data indicate that Ngfr expression discriminates glial cells from MuSCs

169   within a common pool of Itga7+ cells. Indeed, Ngfr+ cells were only detected among the Itga7+

170   population in the muscle at 3 days after denervation, while only a negligible number of Ngfr+ cells

171   were present in control muscle (Figure 3d-e, Suppl. Figure 4a-c). There were no significant changes

172   in the number of Ngfr-Itga7+ cells after nerve injury (Suppl. Figure 4d), thus confirming that the main

173   cell type responding to denervation are the muscle- resident glial cells. Indeed, the number of Pax7+

174   cells did not change at 3 days after nerve injury and Pax7 did not co-localize with Ngfr in serial

175   muscle sections (Suppl. Figure 4e-f). Moreover, the induction of neurotrophic genes, including Ngfr,

176   but also Plp1, Tnc, Nrcam and Gdnf, was only detected in Ngfr+ cells, but not Ngfr- cells, isolated

177   from denervated muscle (Suppl. Figure 4g). Finally, the Ngfr+ cells differed in phenotype and

178   morphology from the Ngfr- population, and unlike the Ngfr- cells, they did not show any myogenic

179   potential when cultured *in vitro* (Suppl. Figure 5a-b).

180   Interestingly, the presence of Ngfr+ cells was also observed in a mouse model of Spinal Cord

181   Injury (SCI) where the damage was induced by mechanical lesion of the spinal cord (Suppl. Figure

182   5c-d). Indeed, at 7 days post spinal lesion, the appearance of Ngfr+ cells was observed in TA muscle.

183   We found that in unperturbed muscles Plp1 positive cells are close to the neuron structure stained

184   for Neurofilament (NF-L) that is lost upon nerve injury. However, upon neve injury, Plp1+ /Ngfr+ cells

185   were found in a structure reminiscent of the nerve structure and close to bungarotoxin-positive NMJs

(Suppl. Figure 4a-c). Moreover, a decline in the number of the Ngfr+ cells and, more importantly, a decrease in the expression of neurotrophic factors was observed at 30 days after nerve injury, when the reinnervation process typically occurs (Suppl. Figure 6a-b).

Activated glial cells are known to respond to nerve injury and participate in nerve repair and axon guidance. To exclude the possibility that the presence of activated glial cells within the muscle was simply caused by co-isolation of adjacent tissues (i.e. nerves), we compared the gene expression profile of Ngfr+ cells isolated from nerves or muscles at 3 days after nerve injury (Figure 4a). Transcriptome analysis revealed significant differences between the two populations, which clearly formed two independent clusters with a large subset of differentially regulated genes (Figure 4a-c). Interestingly, among the genes differentially expressed by the two glial cells we found some genes more represented in muscle derived glial cells (i.e. Tnc, Gdnf), while others are more expressed in neuron derived cells (i.e. Shh) (Figure 4d). We focused on Tnc since its ablation is known to delay NMJ recovery in-vivo(27). Tnc protein unequivocally localized close to bungarotoxin (BTX)-positive NMJ upon denervation (Figure 4e-f and Suppl. Figure 6c). Finally, Tnc protein expression and localization close to the NMJ was observed in TA muscle at 7 days following spinal cord injury (Suppl. Figure 6d).

These results suggest an involvement of Tnc in the maintenance of NMJ following denervation.

Muscle resident glial cells activated by nerve injury adopt a defective neurotrophic phenotype in a mouse model for ALS.

The symptomatic stage of ALS is characterized by muscle denervation. Motoneuron degeneration leads to muscle atrophy and muscle weakness, ultimately accelerating disease progression (28). It is currently unclear whether the disease progression could be influenced by the neurotrophic activity of specialized cell types. We therefore set to determine whether an increased amount of muscle resident Plp1+/Ngfr+ glial cells could be observed at sequential stages of disease progression, using the SOD1^{G93A} mouse model of ALS(29).

213   Indeed, Ngfr expression and Ngfr+ cells among Itga7+ cells increased with disease

214   progression (Figure 5a-d). Ngfr expression displayed a striking increase in muscle derived from

215   symptomatic SOD1^{G93A} at 90- and 140-days of postnatal life with a concomitant reduction of NF-L

216   positive neurofilament in accordance with the progressive loss of muscle innervation (Figure 5b-d).

217   Other factors such as Gdnf or Tenascin C also increased significantly in SOD1^{G93A} in the late stage

218   of the disease (140d) compared to age-matched healthy animals (Figure 5d). Overall, these

219   observations clearly identify muscle glial cells as potential players in the maintenance of nerve to

220   muscle contact in the context of ALS. Interestingly, the magnitude of the induction of Tnc and Gdnf

221   was clearly lower compared to acute denervation shown in Figure 1. This may account for the

222   reduced reinnervation ability of SOD^{G93A} leading to muscle paralysis that marks the end-stage of the

223   disease. In addition to the lower expression of Tnc compared to reversible nerve degeneration, we

224   also observed a marked difference in Tnc localization in ALS muscle. Indeed, while in reversible

225   denervation we observed a clear localization of Tnc protein close to the NMJ, in SOD^{G93A} muscle

226   Tnc signal encircled muscle fibers without the NMJ associated pattern (Figure 5e-f). These data

227   suggest a defect in the response of glial cells during disease progression.

228   To functionally validate the neurotrophic ability of Plp1+Ngfr+ muscle derived glial cells, we

229   utilized an in-vitro transwell system (Figure 6a-c). Ngfr+ and Ngfr- cells were isolated from limb

230   muscle of mice subjected to nerve injury or from symptomatic SOD^{G93A}, and co-cultured with the

231   mouse motor neuron-like hybrid cell line (NSC-34), without direct contact through the use of specific

232   trans-well inserts. Following 72h of co-culture in growth media, Ngfr+ cells from denervated muscle

233   promoted NSC-34 neuronal differentiation when compared to control cells cultured under standard

234   neuronal differentiation conditions, as documented by the increase in neurites length and the mean

235   number of neurites per cell (Figure 6a-c). Conversely, this effect was not observed in NSC-34 co-

236   cultured with Ngfr- cells. Interestingly, a lower ability to promote NSC-34 differentiation and neurite

237   elongation was observed in cells co-cultured with Ngfr+ cells derived from SODG93A muscle (Figure

238   6a-c).

239   These data suggest that an impaired ability of muscle-resident glial cells to adopt a neurotrophic

240   phenotype in response to nerve injury could contribute to progressive loss of NMJ in ALS muscles.

9

241 Next, given the localization of glial cells close to the NMJ, we explored the possibility that they may

242 play a direct role in the promotion and maintenance of NMJ upon denervation. We tested this

243 possibility by using a model of AChR clustering in cultured myotubes, previously described by Ngo

244 and colleagues (30). As shown in Figure 6d-f and in Suppl. Figure7, conditioned media from muscle

245 derived glial cells promote AChR clustering – as revealed by bungarotoxin staining – in differentiated

246 C2C12 myotubes. As a positive control, 4h agrin (Agr) treatment was used. Interestingly, while after

247 a 10' pulse of agrin followed by 4h of release the AChR clustering was reduced, as previously shown

248 (30), replacement of conditioned media after agrin pulse led to a similar induction of AChR clustering

249 compared to a full 4h agrin treatment. These observations support a direct role of muscle glial-

250 released factors in the induction and maintenance of the muscle counterpart of the NMJ. Of note,

251 we the formation of of AChR clustering was much attenuated when using conditioned media by glial

252 cells isolated from the SOD^{G93A} muscle, further suggesting a functional impairment of muscle glial

253 cell function during ALS progression.

254
255 **DISCUSSION**
256
257 scRNAseq-based analysis has been instrumental to unravel the heterogeneity of muscle-

258 resident cells in unperturbed conditions, while highlighting their dynamic transitions through a

259 continuum of functional cellular states and trajectories in response to homeostatic perturbations (22,

260 24, 31–37). These studies have used the typical experimental model of muscle regeneration, by

261 physical injury, which leads to the sequential activation of multiple cell types, to reveal the identity of

262 sub-populations endowed with specialized activities and their coordination in response to

263 regeneration cues. In addition to MuSC activation, scRNAseq analyses has revealed a dramatic

264 expansion and alteration of gene expression profiles in cells from the inflammatory infiltrate

265 immediately after acute muscle injury (24, 34, 37). These cells account for the vast majority of the

266 cell types present in muscles at early time points post injury and establish functional interactions with

267 other cell types within the regenerative environment, including FAPs and MuSCs, to promote

268 myofiber regeneration and injury resolution. As part of the regeneration process, the repair of injured

269 nerve also occurs, although the cellular effectors of this process remain poorly understood. While

270 earlier studies have suggested the potential contribution of MuSCs in the maintenance of NMJ

271   integrity and regeneration (9, 10), the precise identity of the cell types activated by nerve injury and

272   their potential neurotrophic activity remain unknown.

273   Unlike muscle injury, nerve injury does not promote muscle regeneration, but leads to

274   myofiber atrophy and muscle fibrosis (11, 38). These different outcomes are underpinned by

275   differences in activated cell types. For instance, we have previously observed that muscle

276   denervation leads to the selective activation of FAPs, which exhibit transcriptional profiles and

277   biological activities different from FAPs activated in response to acute muscle injury (11, 31).

278   Importantly, denervation does not trigger the massive infiltration of immune cells observed upon

279   muscle injury (11). We argue that the lack of inflammatory infiltrate and the consequent reduction in

280   the amount of inflammatory signals in the milieu of denervated muscles might account for the lack

281   of activation of multiple cell types in denervated muscles (25). At the same time, the selective

282   response of muscles to denervation might help to capture specific muscle-resident cells activated by

283   nerve injury, without the potentially confounding co-existence of other activated cell types.

284   In this study, we describe a population of muscle-resident glial cells that are activated by

285   nerve injury and might contribute to NMJ repair. These cells express Itga7 - a cell surface protein

286   commonly used to prospectively isolate MuSCs (39). Indeed, both previously used FACS strategies

287   and commercial kits could not distinguish the two populations due to the common antigen surface

288   marker. A recent study identified a population of smooth muscle mesenchymal cells (SMMCs) within

289   the FACS-isolated Itga7+ cells that is distinct from MuSCs (22). Interestingly, our results indicate

290   that muscle-resident glial cells, while sharing Itga7 expression with MuSCs and SMMCs, exhibit a

291   distinctive gene expression signature that is enriched in glial cell-specific genes. While some glial

292   lineage-identity marker was constitutively expressed and could be used for their prospective isolation

293   in unperturbed muscles (Plp1), a subset of neurotrophic genes was selectively expressed in these

294   cells only in response to nerve injury. Among them, Ngfr was instrumental to further isolate the

295   fraction of Itga7/Plp1 glial cells activated upon nerve injury (Figure 3). Ngfr is a receptor commonly

296   associated with activated glial cells (40). Since Ngfr expression in Itga7-positive muscle glial cells is

297   only observed upon their activation by nerve injury and coincides with the activation of the

298 neurogenic program, it is conceivable that Ngfr confers upon glial cells the competence to respond

299 to neurogenic signals.

300   Although nerve-associated glial-cells (otherwise defined as Schwann cells) are well known,

301 the biological properties of tissue-resident glial cells have only recently become the object of intense

302 investigation (41).

303   In the case of skeletal muscle, the specific function of peripheral glial cells and their regulation

304 in response to homeostatic perturbations, such as in ALS disease, are currently not well known (19,

305 42). Although several myelinating and non-myelinating cell types (Remak cells and terminal

306 Schwann cells) have been associated with neuron regeneration, a defined molecular signature able

307 to discriminate between subpopulations from different anatomical location and different functional

308 specialization has not been clearly identified. Indeed, the molecular features of terminal Schwann

309 cells remain mostly unknown, because their scarcity has so far impeded a comprehensive analysis

310 (43). Our data indicate that single cell RNA-seq based approaches may circumvent this issue due

311 to their potential to identify transcriptional signatures in a small number of cells within the pool of

312 cells analysed.

313   Our work identified a population of Itga7-expressing cells, distinct from MuSCs and SMMC,

314 that is selectively activated upon nerve injury and adopt a neurogenic gene expression profile and

315 functional neurotrophic properties. Interestingly, activated muscle resident glial cells localize in close

316 proximity to NMJs. While a comparative analysis using the scRNAseq profiles of Ngfr+ cells isolated

317 either from nerves or from muscles at 3 days post nerve injury revealed clear differences in gene

318 expression between these two populations, it is possible that they might represent two different

319 functional states of muscle-resident glial cells. Nevertheless, the differential expression of certain

320 genes, such as Tnc, Gdnf and Shh, suggests that muscle-resident glial cells adopt different

321 functional phenotypes in response to nerve injury.

322   The upregulation of Tnc in muscle-resident glial cells activated by nerve injury has not been

323 shown previously and highlights a fundamental difference between the skeletal muscle response to

324 nerve injury versus myotrauma. In this latter, Tnc is typically expressed by other types of resident-

325 muscle cells (e.g. FAPs) and accumulates within the ECM to regulate MuSC activity (23, 24, 34, 37).

12

326 Conversely, we show that in response to nerve injury, Tnc accumulates in close proximity to

327 bungarotoxin (BTX)-positive NMJ. Thus, higher levels of Tnc in muscle-derived glial cells and its

328 anatomical localization in proximity of NMJ are distinctive features of skeletal muscle response to

329 NMJ injury. Considering that genetic ablation of Tnc causes delay in NMJ recovery in-vivo (27), we

330 speculate that muscle glial-cell derived Tnc could contribute to NMJ repair following injury. This

331 possibility is also supported by the finding that Tnc expression was reduced upon recovery of NMJ

332 integrity (e.g. up to 30 days after lesion). It is possible that transient deposition of Tnc within the ECM

333 at NMJ is an important event to promote NMJ repair and is part of a general program by which

334 muscle glial cells commit to repair injured muscles. Consistently, we found that factors secreted by

335 muscle glial cells could enhance AChR clustering in cultured myotubes.

336   Further studies will be necessary to investigate the actual contribution of muscle glial cells in

337 the recovery of NMJ integrity in response to acute lesions or chronic degeneration, and whether

338 these cells might be amenable to pharmacological manipulation to facilitate nerve repair. In this

339 regard, pharmacological activation of the neurotrophic potential of muscle glial cells could be

340 exploited in neurodegenerative disorders, such as ALS. A role for peripheral glial cells in ALS – and

341 in particular pre-synaptic Schwann cells - has been recently suggested, although the precise

342 mechanism of their involvement remains unknown (42, 44). We found a progressive increase of

343 muscle resident glial cells in muscles of the ALS mouse model - SOD1^{G93A} mice. However, activated

344 muscle glial cells from symptomatic SOD1^{G93A} mice exhibited reduced activation of neurotrophic

345 genes, defective Tnc localization, impaired ability to promote neurite outgrowth/differentiation of a

346 motoneuron cell line and to promote AChR clustering in cultured myotubes, as compared to glial

347 cells activated in the context of acute reversible denervation. These data suggest that defective

348 activity of muscle-glial cells could contribute to the pathogenesis of neurodegenerative diseases,

349 such as ALS.

350

351

352

METHODS

Mouse Strains

Mouse strains used in this study were:

- C57BL/6J were provided by the Jackson Laboratory (Bar Harbor, USA).

- PAX7CreER/tdTomato[f/f] mice were provided by the SBP Animal Facility (La Jolla).

- Hemizygous transgenic mice carrying the mutant human SOD1[G93A](B6.Cg-Tg (SOD1*G93A)1Gur/J) gene were originally obtained from Jackson Laboratories (Bar Harbor, USA).

- CD1 were provided by Charles River Laboratories, Como, Italy.

All mice were maintained in a pathogen-free animal facility under standard 12h light/12h dark cycle at 21 °C with access to red house and to standard chow and water ad libitum. Three-month-old mice were used for ex-vivo experiments, except for the SOD1[G93A] mice, as indicated in the Figure 5. For the denervation experiments, both male and female C57BL/6J and PAX7CreER/tdTomato[f/f] mice were used. Only female mice were used for the spinal cord injury experiment. As a mouse model of ALS male SOD1[G93A] mice were used.

Cell Lines and Primary Cell Cultures

All cells were cultured in incubators at 37 °C and 5% CO_2. We used mouse MN-like NSC-34 cells (obtained from ATCC) which is a hybrid cell line produced by the fusion of MNs from the spinal cord embryos with N18TG2 neuroblastoma cells that exhibit properties of MNs after differentiation and maturation protocols(45). Thus, NSC-34 cells were grown in proliferation media [Dulbecco's Modified Eagle Medium: Nutrient Mixture *F-12* (*DMEM / F-12*, Sigma-Aldrich, D6421) supplemented with 10% of fetal bovine serum (FBS, Sigma, F4135) and 1% of Penicillin/Streptomycin (Gibco, 15070-063)]. Differentiation was induced by changing medium for DMEM-F12 plus 0.5% of FBS, 1% of non-essential amino acids (NEAA, Thermo Fisher Scientific, 11140050), 1% of Penicillin/Streptomycin.

14

Freshly isolated MuSCs and Ngfr+ cells were plated in 24-well plates in GM [DMEM [+Pyruvate] (Gibco, 41966-029), 20% FBS, 10% Hourse Serum, 1% Chick Embryo Extract (CEE)]. Myogenic differentiation was induced with DMEM and 2% horse serum for 2 or 3 days. NSC-34 and Ngfr+ cells were also used for co-culture experiments.

C2.12 (C2C12) myogenic cells were obtained from ATCC and cultured on 96-well plates in growth medium [DMEM [-Pyruvate] (Gibco, 61965-026), supplemented with 10% of FBS and 1% of Penicillin/Streptomycin]. Myogenic differentiation was induced by shifting the cells in differentiation medium (DMEM [-Pyruvate] complemented with 1% Penicillin/Streptomycin and 2% House Serum).

Acetylcholine receptor clustering assay

AChRs were considered to be a large AChR cluster when they were ≥ 25 μm in their longest dimension. C2C12 myotube were treated with 1 nM recombinat Rat Agrin (R&D System, 550-AG) for 4 hours or 10 minutes in differentiation medium (30). Different C2C12 myotube cultures were treated with conditioned media of muscle derived glial cells for 4h or after the 10' pulse of agrin. AChRs were labeled by the binding of Alexa Fluor 488 α-bungarotoxin (Invitrogen, B13422). Myotubes were incubated with the α-bungarotoxin diluted (1:300) in differentiation medium for 1 hours at 37°C in 5% CO_2. The number of AchR clusters per field in their longest dimension (≥ 25 μm) was measured by ImageJ.

Denervation

Unilateral hindlimb denervation was performed by clamping the left sciatic nerve under anesthesia by intraperitoneal injection of 40 mg/kg ketamine (Zoletil®, Virbac) and 10 mg/kg xylazine (Rampum, BAYER). Upon exposure of the sciatic nerve, the nerve was crushed for three times for 10 seconds. Alternative, for the bulk RNA-seq in Figure1a, nerve was cut with a scissor. The lesion was sutured after the operation.

Spinal cord injury

Three-month-old CD1 mice were used in SCI. To perform SCI, mice were deeply anaesthetized with a mixture 1:1 of Rompun (Bayer 20 mg ml^{-1}; 0.5 ml kg^{-1}) and Zoletil (100 mg ml^{-1}; 0.5 ml kg^{-1}), the back hairs were shaved, the skin was disinfected with betadine, and an incision was made to expose the spinal cord. Animals were mounted on a stereotaxic apparatus with spinal adaptors connected to a cortical PinPoint precision impactor device (Stoelting) and maintained at 37 °C throughout surgery. To induce a severe trauma the following parameters were set up: middle, round and flat tip (#4); velocity 3 m s^{-1}; depth 5 mm; dwell time 800 ms. The impact was applied at the thoracic level (vertebrae T10–T11). Analysis of the graphical impact parameters, operated by the PinPoint software, was used to identify potential outliers. Behavioural analyses were also used to corroborate differences in injury severity within groups. Slight lesions were excluded from the study based on these criteria.

Cell preparation and isolation by FACS

Tibialis anterior and gastrocnemius muscles, or nerves, of mice were subjected to enzymatic dissociation [in PBS with 2 mg/mL Collagenase A (Roche, 10 103 586 001), 2,4 U/mL Dispase I (Roche, 04 942 078 001), 10 ng/mL DNase (Sigma, 11 284 932 001), 0,4 mM CaCl$_2$ and 5mM MgCl$_2$] for 60 min at 37° C. The cell suspension was filtered through a 40-μm nylon filter and incubated with the following antibodies for 30 min: CD45 (Invitrogen, 48-0451-82), CD31 (Invitrogen, 48-0311-82), TER119 (Invitrogen, 48-5921-82), Sca1 (Invitrogen, 11-5981-82) and Itga7 (AbLab, R2F2), Ngfr (Miltenyi Biotec, 130-118-793).

Ngfr+ cells were isolated as TER119−/CD45−/CD31−/Itga7+/SCA-1−/Ngfr+ cells and Pax7-Tomato + as TER119−/CD45−/CD31−/Itga7+/SCA-1−/Tomato+ (Suppl.Figure1b).

In Suppl.Figure1a, satellite cell purification was performed by using SC Isolation Kit (Miltenyi Biotech, Bergisch Gladbach, Germany, 130-104-268).

Histology Immunofluorescence

For the histological analysis 8 μm muscle cryosection were analysed. Both cryosections and cultured cells were fixed in 4% PFA (Sigma, P6148) for 10 min and permeabilized with 100% acetone for 1 min at RT or with 0.1% Triton for 15 min at RT. Muscle sections and cultured cells were then blocked for 1h with a solution containing 4% BSA (Sigma, A7030-100G) in PBS. PAX7 staining was performed by an antigen retrieval protocol. The primary antibodies immunostaining was performed ON at 4°C and then the antibody binding specificity was revealed using secondary antibodies coupled to Alexa Fluor 488, 594, or 647 [Invitrogen, Goat anti-Mouse Alexa Flour 647 (1:400, A32728), Goat anti-Rabbit Alexa Flour 488 (1:400, A32731), Goat anti-Mouse Alexa Flour 488, (1:400, A32723)]. Acetylcholine receptors (AChRs) were revealed with fluorescently labeled Bungarotoxin (BTX) (1:500 Alexa 594, Invitrogen, B13423). Sections were incubated with DAPI (Thermo Fisher Scientific, D1306) in PBS for 5 minutes for nuclear staining, washed in PBS, and mounted with glycerol (3:1 in PBS).

The primary antibodies used for immunofluorescences are: rabbit anti-Plp1 (1:100, Cell Signaling, 28702S); mouse anti NFl (1:200, Santa Cruz Biotechnology, SC-20012); rat anti-Ngfr-PE (1:100, Miltenyi Biotec, 130-118-793); rabbit anti-Tnc (1:100, EMD Millipore Corp, AB19013); mouse anti-Caveolin-3 (1:1000, BD Transduction Laboratories, 610420); rabbit anti-Laminin (1:400, Sigma, L9393); anti BIII Tubulin mAb (1:500, PROMEGA, G712A); mouse anti-PAX7 (1:20, Developmental Studies Hybridoma Bank DSHB, Pax7); mouse anti-Myosin (1:10, Developmental Studies Hybridoma Bank DSHB, MF20); mouse α-Tubulin (1:200, Cell Signaling, #2144).

The transverse sections and cultured cells were visualized on a Zeiss confocal microscope then edited using the ImageJ® software. All histological analyses were performed in a blinded fashion. The figures reported are representative of all the examined fields.

EdU Proliferation Assay

Cell proliferation was measured by EdU incorporation. 20 mg per kg body weight EdU was administered intraperitoneally (i.p.) 12h before muscle harvest. Incorporation of EdU was revealed

463　using the "Click-iT™ EdU Cell Proliferation Kit for Imaging, Alexa Fluor™ 594 dye" (Thermo Fisher

464　Scientific, C10354) following the manufacture protocol.

465

466　**Co-culture conditions of Ngfr+ cells and NSC34**

467　NSC-34 and Ngfr+ cells were cocultured by using inserts with 1µm porous membrane to avoid direct

468　contact between populations. NSC-34 were grown independently from Ngfr+ in proliferation media

469　for 48h in 24-well plates. After 24h, freshly sorted Ngfr+ cells were plated on the upper insert and

470　transwell co-cultures were maintained for additional 72h in proliferation and differentiation media.

471

472　**RNA analysis by quantitative PCR**

473　RNA was extracted from cells using Qiagen RNeasy mini-kits (Qiagen, 74106) following the

474　manufacturer's protocol. Total RNA was quantified with a Nanodrop 8000 spectrophotometer

475　(Thermo Scientific, Wilmington). First-strand cDNA was synthesized from total RNA using the

476　Transcriptor First Strand cDNA Synthesis kit (Roche, N808-0234) following the manufacturer's

477　protocols. The generated cDNA was used as a template in real-time PCR reactions with 2x Fast Q-

478　PCR Master Mix (SYBR, ROX) (SMOBIO, TQ1211) and was run on a Roche LC480 machine using

479　three-step amplification and melt curve analysis. Quantitative real-time PCR reactions consisted of

480　2× SYBR Green Supermix, 0.25 μmol l^{-1} forward and reverse primers and 10 ng cDNA. Relative

481　gene expression was normalized by dividing the specific expression value by the glyceraldehyde 3-

482　phosphate dehydrogenase (Gapdh) expression value and calculated using the $2^{-\delta\Delta CT}$ method.

483　The following primer sets were used to identify transcripts:

484　Gapdh FW: CACCATCTTCCAGGAGCGAG, Gapdh RV: CCTTCTCCATGGTGGTGAAGAC,

485　Ngfr FW: TGCCTGGACAGTGTTACGTT, Ngfr RV: ACAGGGAGCGGACATACTCT,

486　Shh FW: CACCCCCAATTACAACCCCG, Shh RV: CTTGTCTTTGCACCTCTGAGTC,

487　Fgf5 FW: CTGTACTGCAGAGTGGGCAT, Fgf5 RV: AATTTGGCTTAACACACTGGC,

488　Runx2 FW: GCCTTCAAGGTTGTAGCCCT, Runx2 RV: GTTCTCATCATTCCCGGCCA,

489　Olig1 FW: CTCGCCCAGGTGTTTTGTTG, Olig1 RV: TAAGTCCGAACACCGATGGC,

490　Tnc FW: CTACCACAGAGGCCTTGCC, Tnc RV: AGCAGCTTCCCAGAATCCAC,

18

491 Pax7 FW: AGGACGACGAGGAAGGAGACA, Pax7 RV: TCATCCAGACGGTTCCCTTT

492 Vcam1 FW: GCACTCTACTGCGCATCTT, Vcam1 RV: CACCAGACTGTACGATCCT

493 Nrcam FW: ATGCACAGACATCAGTGGGG, Nrcam RV: GCTTGCCATTGCCTTCTTACC

494 Gdnf FW: TGGGTCTCCTGGATGGGATT, Gdnf RV: CGGCGGCACCTCGGAT

495 Rgs5 FW: CGCACTCATGCCTGGAAAG, Rgs5 RV: TGAAGCTGGCAAATCCATAGC

496 Myl9 FW: GCGCCGAGGACTTTTCTTCT, Myl9 RV: CCTCGTGGATGAAGCCTGAG

497 Plp1 FW: CCTAGCAAGACCTCTGCCAGTA, Plp1 RV: GGACAGAAGGTTGGAGCCACAA

498

499 **Tamoxifen (Tmx) treatment and denervation**

500 We used PAX7CreER/tdTomato$^{f/f}$ mice between the ages of 2 and 3 mouth for Tmx (Sigma, T5648)

501 injections. Tmx (3 mg) suspended in corn oil was injected intraperitoneally (i.p.) each day for 5 d.

502 After 7 d from the last injection, we performed the unilateral hindlimb denervation. Tissues were

503 harvested after 3 d for FACS.

504

505 **RNA-sequencing**

506 MuSC were isolated from mice TA and GA muscle as described. RNA from MuSC was extracted

507 using RNeasy Mini kit (Qiagen) following the manufacturer's protocol. RNA was shipped to the

508 sequencing IGA of Udine. The libraries for sequencing were prepared using NuGEN Ovation System

509 V2 RNA-Seq. For each biological sample two independent experiments were carried out for the

510 isolation of RNA. All duplicates are pool of three different mice, sorted at different times.

511

512 **RNA-sequencing data processing**

513 For sequencing alignment we used the mouse reference genome assembly GRCm38/mm10

514 (http://ftp.ensembl.org/pub/release-76/fasta/ mus_musculus/dna/), and for transcriptome annotation

515 we used version 85 of the GRCm38

516 (http://ftp.ensembl.org/pub/release85/gtf/mus_musculus/Mus_musculus. GRCm38.85.gtf.gz). We

517 used the FASTQC package (v0.11.3) to assess the quality of sequenced libraries. All passed quality

518 control. Reads were mapped to the reference genome using TopHat2 v.2.1.1. The quality control of

519   the reads distribution along transcripts was performed using infer_experiment.py from RSeQC

520   package v2.6.3. All samples had a uniform distribution of reads along transcripts. The sequenced

521   read counts per annotated gene were derived with the use of htseq-count script distributed with

522   HTSeq v0.5.4p5. We used the R library package DESeq2 v.1.12.4 for measuring differential gene

523   expression between two different cell conditions, considering the two RNA–seq experiments as

524   biological replicates. We picked genes with adjusted P value < 0.001. Gene ontology analysis was

525   performed using David 6.8 (https://david.ncifcrf.gov/). In details Biological Process was predicted on

526   genes differentially expressed with p adjusted<0.01 with the following setting: threshold counts=2,

527   threshold EASE=0.1. The most significant 12 functional annotation was illustrated in the figure.

528

529   **Single-cell RNA-sequencing**

530   Single-cell RNA-sequencing was performed at IGA facility of Udine - Italy

531   (https://igatechnology.com/). Methanol fixed cells were rehydrated following 10X Genomics

532   recommendation. In order to remove visible debris, an additional washing in Wash-Resuspension

533   buffer was introduced. Cell concentration was determined using the Countess II FL Automated Cell

534   Counter (Thermo Fisher Scientific, Waltham, MA). Trypan Blue staining of the methanol fixed cells

535   showed that 100% of the cells were dead, indicating that all cells were effectively fixed and

536   permeabilized.

537   Chromium controller and Chromium NextGEM Single Cell 3' Reagents Kit v3.1 (10X Genomics,

538   Pleasanton, CA) have been used for partitioning cells into Gel Beads-in-emulsion (GEMs), where all

539   generated cDNA share a common 10x barcode. Libraries were generated from the cDNA following

540   manufacturer's instruction and checked with both Qubit 2.0 Fluorometer (Invitrogen, Carlsbad, CA)

541   and Agilent Bioanalyzer DNA assay (Agilent technologies, Santa Clara, CA). Libraries were then

542   prepared for sequencing and sequenced on NovaSeq6000 (Illumina, San Diego, CA) with the

543   following run parameters: Read 1=28 cycles, i7 index=8 cycles, Read 2=91 cycles.

544

545

546

Single-cell RNA-sequencing data processing.

The raw sequencing data were processed by Cell Ranger v 3.1.0 (10X Genomics) with mouse transcriptome reference mm10 to generate gene-cell expression matrices. Further data analysis was carried out in R version 3.6.0 using Seurat version 3.1.1(46). The two datasets were set up as independent Seurat objects. ''Cells'' that fit any of the following criteria were filtered out: < 200 or > 4,500 expressed genes, or > 10% UMIs mapped to mitochondria. Dataset normalization and identification of variable features were performed using the NormalizeData() function and the FindVariableFeatures() with following parameters (selection.method = "vst", nfeatures = 4000). Integration anchors were computed using the first 20 dimensions, using all the genes present in both datasets as features to integrate. Finally, we obtained 3949 cells that passed quality control, with an average of 1,460 genes expressed per cell. For downstream integrated analyses, top 30 components were used for PCA, UMAP and cluster identification (using a resolution of 0.4). Further, we manually assigned cell population identity based on cell-type-specific markers and merged those clusters that displayed similar canonical markers. After clustering and cell population identification, the most highly differentially expressed genes, or putative cluster markers, were identified by a likelihood-ratio test using the FindAllMarkers() function with the following parameters(only.pos = TRUE, min.pct =0.5, min.diff.pct=0.25, logfc.threshold = 0.25). Genes differentially expressed in CTR vs DEN where identified using the FindMarkers() function and subsequently filtered using the following criteria (pct.1>0.45 or pct.2>0.45; p_val_adj<0.01; avg_logFC< (-0.58) or avg_logFC>0.58). Dataset Integration with previously published scRNAseqs (Giordani and De Micheli) has been performed in Seurat with FindIntegrationAnchors() and IntegrateData() functions using the first 20 dimensions. From the De Micheli dataset, only the uninjured datapoint ("D0") has been used for comparison. Both datasets were downloaded from the GEO website.

Figure Design

Graphical abstract, Figure 1d, Figure 4a, Figure 6b and Figure 6e were created with BioRender (https://biorender.com/)

Statistics

Data are presented as mean with SD. Statistical analysis was performed using Graph Pad Prism 8.0 software (Pad Software). Normality was tested by Shapiro-Wilk test. Unpaired, two-tailed Student's t test was used to compare the means of two parametric groups, while Mann-Whitney test for two non-parametric groups. One-way ANOVA with Tukey's post-test was used for comparison among the different parametric data sets. Significance was defined as $P < 0.05$ (*), $P < 0.01$ (**), and $P < 0.001$ (***).

The number of biological replicates for each experiment is indicated in the figure legends. RNAseq data was performed in 2 independent samples derived from different animals. Statistical method was Deseq2. Right-tailed Fisher's exact test and one-sided Fisher's exact test was used for IPA analyses. For scRNA-seq, biological sample replicates came also from separate mice. Histological and Immunofluorescence images are representative of at least 3 different experiment/animals. For cell culture studies, biological replicates from separate culture wells.

Data and code availability

a7int+ mouse bulk RNA-sequencing data, Mouse Single Cells RNA-sequencing data and Ngfr+ Mouse bulk RNA-sequencing data are available at the SRA repository (Accession numbers: PRJNA623246, PRJNA626530 and PRJNA649152).

STUDY APPROVAL

All experiments in this study were performed in accordance with protocols approved by the Italian Ministry of Health, National Institute of Health (IIS), and Santa Lucia Foundation (Rome) and by the Sanford Burnham Prebys Medical Discovery Institute Animal Care and Use Committee. The study is compliant with all relevant ethical regulations regarding animal research and in the respect of the principles of the 3Rs (Replacement, Reduction and Refinement).

REFERENCES

1. Farup J, Madaro L, Puri PL, Mikkelsen UR. Interactions between muscle stem cells,

mesenchymal-derived cells and immune cells in muscle homeostasis, regeneration and disease.

Cell Death Dis. 2015;6(7):e1830–e1830.

2. Bentzinger CF, Wang YX, Dumont NA, Rudnicki MA. Cellular dynamics in the muscle satellite

cell niche. *EMBO Rep.* 2013;14(12):1062–1072.

3. Mauro A. Satellite cell of skeletal muscle fibers. *J Biophys Biochem Cytol* 1961;9:493–495.

4. Woszczyna MN, Rando TA. A Muscle Stem Cell Support Group: Coordinated Cellular Responses

in Muscle Regeneration. *Dev Cell* 2018;46(2):135–143.

5. Feige P, Brun CE, Ritso M, Rudnicki MA. Orienting Muscle Stem Cells for Regeneration in

Homeostasis, Aging, and Disease. *Cell Stem Cell* 2018;23(5):653–664.

6. Baghdadi MB, Tajbakhsh S. Regulation and phylogeny of skeletal muscle regeneration. *Dev.*

Biol. 2018;433(2):200–209.

7. García-Prat L, Sousa-Victor P, Muñoz-Cánoves P. Proteostatic and Metabolic Control of

Stemness. *Cell Stem Cell* 2017;20(5):593–608.

8. Brack AS, Rando TA. Tissue-specific stem cells: lessons from the skeletal muscle satellite cell..

Cell Stem Cell 2012;10(5):504–14.

9. Liu W, Wei-LaPierre L, Klose A, Dirksen RT, Chakkalakal J V. Inducible depletion of adult

skeletal muscle stem cells impairs the regeneration of neuromuscular junctions. *Elife* 2015;4.

doi:10.7554/eLife.09221

10. Liu W et al. Loss of adult skeletal muscle stem cells drives age-related neuromuscular junction

degeneration. *Elife* 2017;6. doi:10.7554/eLife.26464

11. Madaro L et al. Denervation-activated STAT3-IL-6 signalling in fibro-adipogenic progenitors

promotes myofibres atrophy and fibrosis. *Nat Cell Biol* 2018;20(8):917–927.

12. Sakaguchi S et al. Implication of anti-inflammatory macrophages in regenerative moto-

neuritogenesis: Promotion of myoblast migration and neural chemorepellent semaphorin 3A

expression in injured muscle. *Int. J. Biochem. Cell Biol.* 2014;54:272–285.

13. Tatsumi R et al. Possible implication of satellite cells in regenerative motoneuritogenesis: HGF

648   upregulates neural chemorepellent Sema3A during myogenic differentiation. *Am. J. Physiol. - Cell*

649   *Physiol.* 2009;297(2). doi:10.1152/ajpcell.00161.2009

650   14. Pradat PF et al. Abnormalities of satellite cells function in amyotrophic lateral sclerosis.

651   *Amyotroph Lateral Scler* 2011;12(4):264–271.

652   15. Scaramozza A et al. Skeletal muscle satellite cells in amyotrophic lateral sclerosis. *Ultrastruct*

653   *Pathol* 2014;38(5):295–302.

654   16. Sandri M. Protein breakdown in muscle wasting: role of autophagy-lysosome and ubiquitin-

655   proteasome. *Int J Biochem Cell Biol* 2013;45(10):2121–2129.

656   17. Glass DJ. Signalling pathways that mediate skeletal muscle hypertrophy and atrophy. *Nat. Cell*

657   *Biol.* 2003;5(2):87–90.

658   18. Braun T, Gautel M. Transcriptional mechanisms regulating skeletal muscle differentiation,

659   growth and homeostasis. *Nat. Rev. Mol. Cell Biol.* 2011;12(6):349–361.

660   19. Li L, Xiong W-C, Mei L. Neuromuscular Junction Formation, Aging, and Disorders. *Annu. Rev.*

661   *Physiol.* 2018;80(1):159–188.

662   20. Tiwari N et al. Stage-Specific Transcription Factors Drive Astrogliogenesis by Remodeling

663   Gene Regulatory Landscapes.. *Cell Stem Cell* 2018;23(4):557-571.e8.

664   21. Magill CK et al. Reinnervation of the tibialis anterior following sciatic nerve crush injury: a

665   confocal microscopic study in transgenic mice. *Exp Neurol* 2007;207(1):64–74.

666   22. Giordani L et al. High-Dimensional Single-Cell Cartography Reveals Novel Skeletal Muscle-

667   Resident Cell Populations. *Mol. Cell* 2019;74(3):609-621.e6.

668   23. Tierney MT et al. Autonomous Extracellular Matrix Remodeling Controls a Progressive

669   Adaptation in Muscle Stem Cell Regenerative Capacity during Development. *Cell Rep.*

670   2016;14(8):1940–1952.

671   24. De Micheli AJ et al. Single-Cell Analysis of the Muscle Stem Cell Hierarchy Identifies

672   Heterotypic Communication Signals Involved in Skeletal Muscle Regeneration. *Cell Rep.*

673   2020;30(10):3583-3595.e5.

674   25. Nicoletti C et al. scRNA-seq-based analysis of skeletal muscle response to denervation reveals

675   selective activation of muscle-resident glial cells and fibroblasts. *bioRxiv* 2020;2020.12.29.424762.

676   26. Hicks MR et al. ERBB3 and NGFR mark a distinct skeletal muscle progenitor cell in human

677   development and hPSCs. *Nat Cell Biol* 2018;20(1):46–57.

678   27. Cifuentes-Diaz C et al. Abnormal reinnervation of skeletal muscle in a tenascin-C-deficient

679   mouse. *J. Neurosci. Res.* 2002;67(1):93–99.

680   28. Kiernan MC et al. Amyotrophic lateral sclerosis. In: *The Lancet*. Elsevier; 2011:942–955

681   29. Tu PH et al. Transgenic mice carrying a human mutant superoxide dismutase transgene

682   develop neuronal cytoskeletal pathology resembling human amyotrophic lateral sclerosis lesions.

683   *Proc. Natl. Acad. Sci. U. S. A.* 1996;93(7):3155–3160.

684   30. Ngo ST, Cole RN, Sunn N, Phillips WD, Noakes PG. Neuregulin-1 potentiates agrin-induced

685   acetylcholine: Receptor clustering through muscle-specific kinase: Phosphorylation. *J. Cell Sci.*

686   2012;125(6):1531–1543.

687   31. Malecova B et al. Dynamics of cellular states of fibro-adipogenic progenitors during

688   myogenesis and muscular dystrophy. *Nat Commun* 2018;9(1):3670.

689   32. Der Vartanian A et al. PAX3 Confers Functional Heterogeneity in Skeletal Muscle Stem Cell

690   Responses to Environmental Stress. *Cell Stem Cell* 2019;24(6):958-973.e9.

691   33. Dell'Orso S et al. Single cell analysis of adult mouse skeletal muscle stem cells in homeostatic

692   and regenerative conditions. *Development* 2019;146(12):dev174177.

693   34. Oprescu SN, Yue F, Qiu J, Brito LF, Kuang S. Temporal Dynamics and Heterogeneity of Cell

694   Populations during Skeletal Muscle Regeneration. *iScience* 2020;23(4).

695   doi:10.1016/j.isci.2020.100993

696   35. Schaum N et al. Single-cell transcriptomics of 20 mouse organs creates a Tabula Muris

697   [Internet]. *Nature* 2018;562(7727):367–372.

698   36. Scott RW, Arostegui M, Schweitzer R, Rossi FMV, Underhill TM. Hic1 Defines Quiescent

699   Mesenchymal Progenitor Subpopulations with Distinct Functions and Fates in Skeletal Muscle

700   Regeneration. *Cell Stem Cell* 2019;25(6):797-813.e9.

701   37. Pawlikowski B et al. A cellular atlas of skeletal muscle regeneration and aging. *bioRxiv*

702   2019;635805.

703   38. Rebolledo DL et al. Denervation-induced skeletal muscle fibrosis is mediated by CTGF/CCN2

704   independently of TGF-β. *Matrix Biol.* [published online ahead of print: February 2019];

705   doi:10.1016/J.MATBIO.2019.01.002

706   39. Pasut A, Jones AE, Rudnicki MA. Isolation and culture of individual myofibers and their satellite

707   cells from adult skeletal muscle. *J. Vis. Exp.* 2013;(73):e50074.

708   40. Jessen KR, Mirsky R. The origin and development of glial cells in peripheral nerves. *Nat. Rev.*

709   *Neurosci.* 2005;6(9):671–682.

710   41. Carr MJ et al. Mesenchymal Precursor Cells in Adult Nerves Contribute to Mammalian Tissue

711   Repair and Regeneration. *Cell Stem Cell* 2019;24(2):240-256.e9.

712   42. Lasiene J, Yamanaka K. Glial cells in amyotrophic lateral sclerosis. *Neurol. Res. Int.*

713   2011;2011. doi:10.1155/2011/718987

714   43. Alvarez-Suarez P, Gawor M, Prószyński TJ. Perisynaptic schwann cells - The multitasking

715   cells at the developing neuromuscular junctions. *Semin. Cell Dev. Biol.* 2020;104:31–38.

716   44. Arbour D, Vande Velde C, Robitaille R. New perspectives on amyotrophic lateral sclerosis: the

717   role of glial cells at the neuromuscular junction. *J. Physiol.* 2017;595(3):647–661.

718   45. Cashman NR et al. Neuroblastoma × spinal cord (NSC) hybrid cell lines resemble developing

719   motor neurons. *Dev. Dyn.* 1992;194(3):209–221.

720   46. Stuart T et al. Comprehensive Integration of Single-Cell Data. *Cell* 2019;177(7):1888-

721   1902.e21.

722
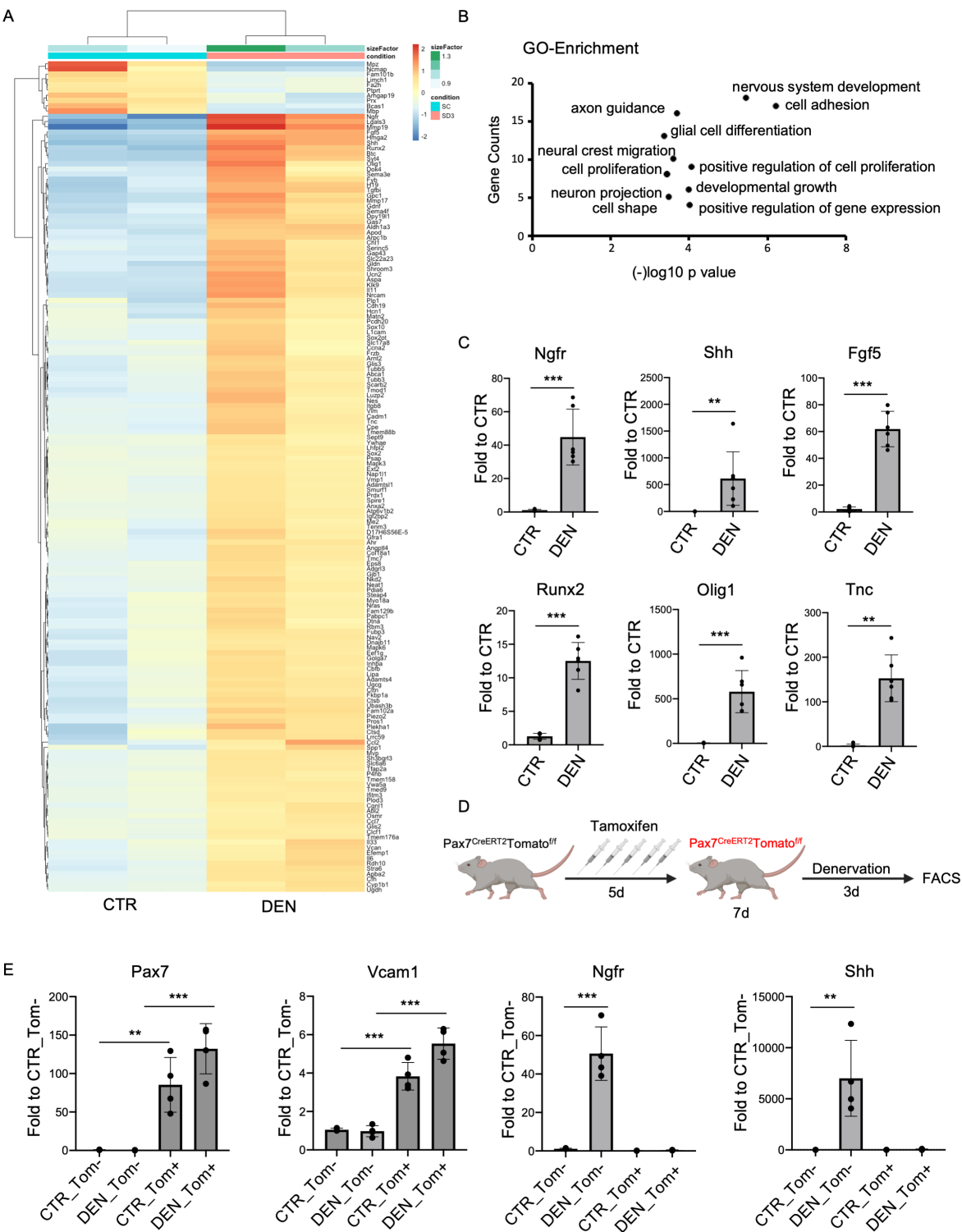
Figure 1. Activation of a neurotrophic signaling pathway in the Itga7+Sca1-Ln- myogenic cell fraction.

A) Heatmap representation of genes significantly deregulated - p adj<0.001 - in Itga7+Sca1-Ln- freshly isolated cells derived from denervated (cut) muscle at 3-days post nerve lesion (n=2). **B)** GO-Enrichment in Biological Function (BF) of genes significantly deregulated - p adj<0.001 - in Itga7+Sca1-Ln- cells derived from at 3 days denervated muscle. **C)** qPCR analysis for the expression of Ngfr, Shh, Fgf5, Runx2, Olig1 and Tnc in freshly isolated Itga7+Sca1-Ln- cells derived from control and 3 days reversible denervated (crush) muscle. Gapdh was used as housekeeping gene (n≥5, Values represent mean ± s.d. **P < 0.01 and ***P < 0.001; by student t-test (Ngfr, Fgf5, Olig1, Runx2, Shh) or by Mann-Whitney test (Tnc)). **D)** Working model of tamoxifen induced in-vivo treatment. **E)** qPCR analysis for the expression of Pax7, Vcam1, Ngfr and Shh in freshly isolated Tomato+ and Tomato- cells derived from control and 3 days denervated muscle of tamoxifen treated PAX7.Cre_tdTomato mice. Gapdh was used as housekeeping gene (n=4, Values represent mean ± s.d. **P < 0.01 and ***P < 0.001; by One Way Anova Tukey's Multiple Comparisons test).
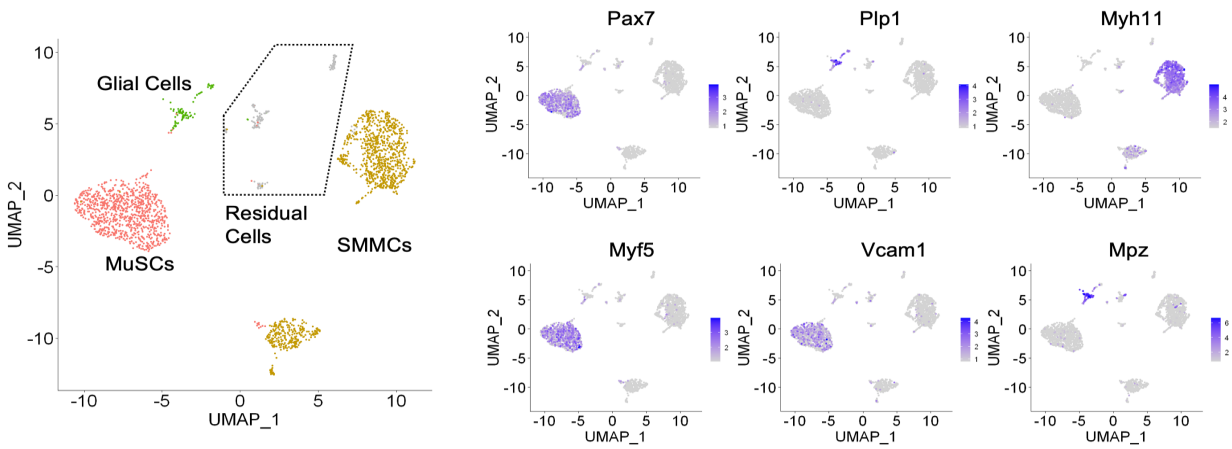
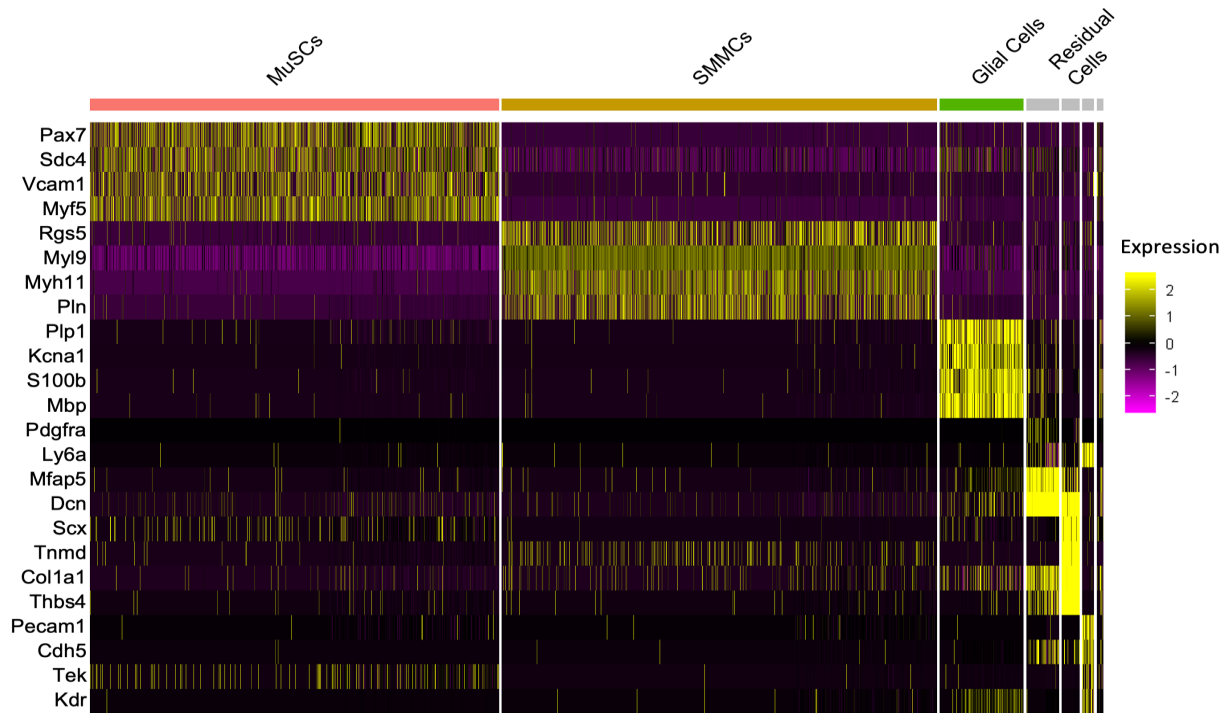**Figure 2. Itga7+ cell heterogeneity revealed by scRNA-seq analysis.**

743 **A)** Distribution of Pax7, Plp1, Myh11, Myf5, Vcam1 and Mpz transcripts in Uniform Manifold

744 Approximation and Projection (UMAP)-derived clusters of single cells (Single Cells RNA-seq) of

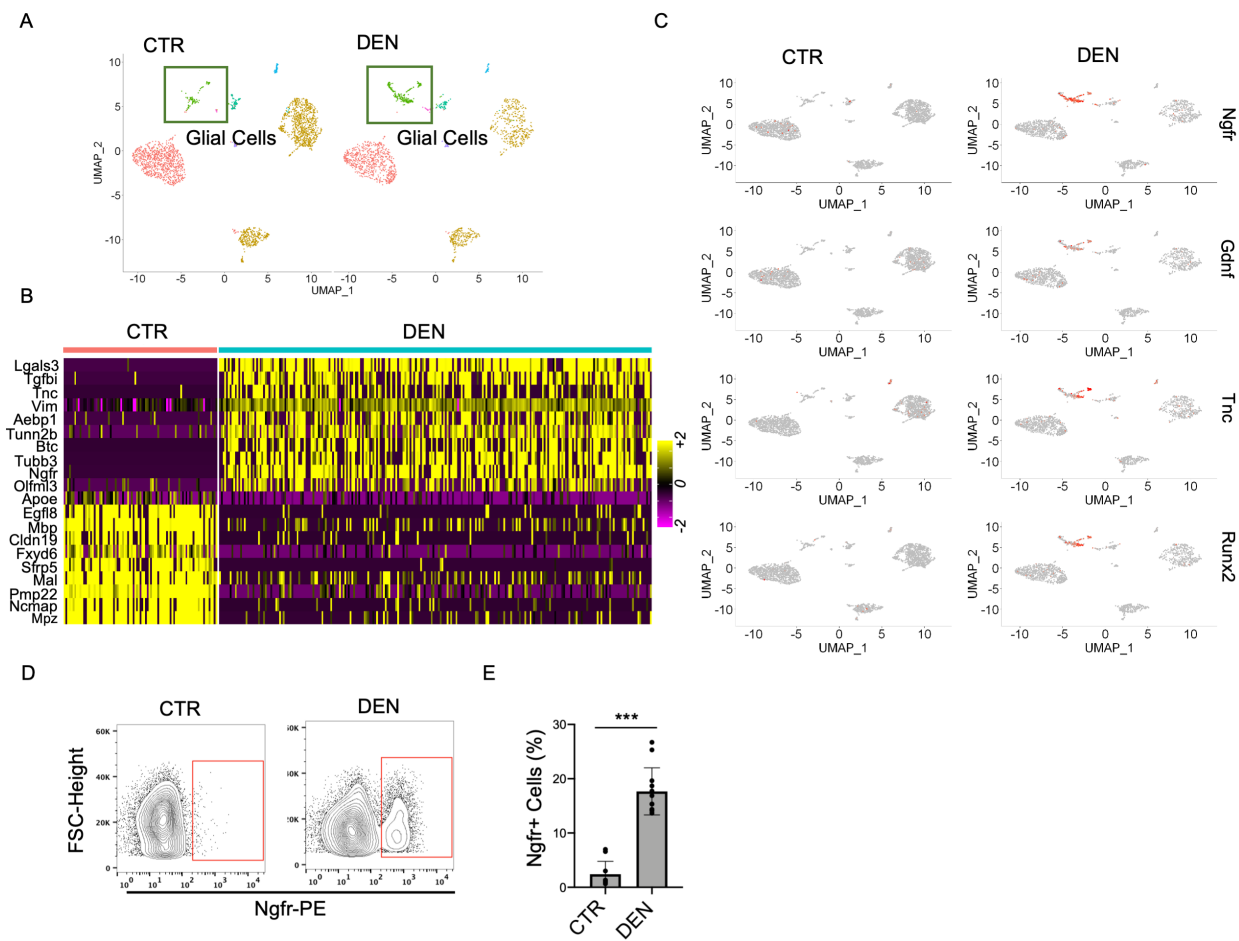745 Itga7+Sca1-Ln- isolated cells from control muscle. **B)** RNA expression heatmap for the given cell

746 populations (column) and genes (row), sorted by clusters. The canonical markers used to identify

747 each cluster are plotted (or the most variable genes per cluster in cases where markers were not

748 already present in the literature).

749

752 **Figure 3. Activation of a neurotrophic signalling pathway in muscle glial cells upon**
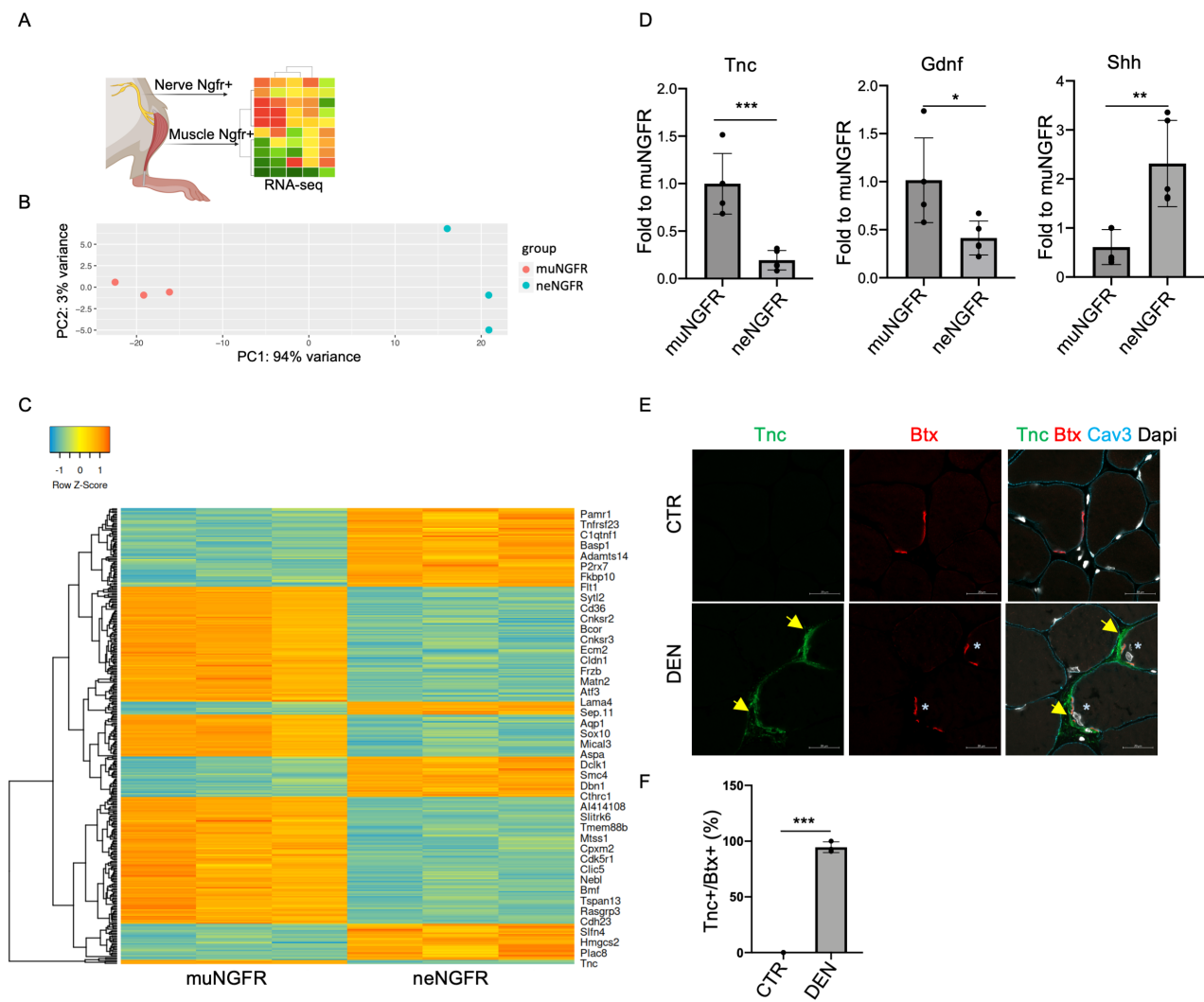
753 **denervation.**

754 **A)** Distribution in Uniform Manifold Approximation and Projection (UMAP)-derived clusters of single

755 cells (Single Cells RNA-seq) of Itga7+Sca1-Ln- isolated cells from control (CTR-left) and 3-days

756 denervated muscle (DEN-right). **B)** RNA expression heatmap for Plp1 cell populations isolated from

757 control and denervated muscle (row) and genes (column), sorted by clusters. **C)** Distribution of Ngfr,

758 Gdnf, Tnc and Runx2 transcripts in Uniform Manifold Approximation and Projection (UMAP)-derived

759 clusters of single cells (Single Cells RNA-seq) of Itga7+Sca1-Ln- isolated cells from control (left) and

760 denervated (right) muscle. **D)** Representative cytofluorimetric plot of Ngfr+ - gated within the

761 Itga7+Sca1-Ln- population - cells in control (left) and denervated (right) muscle. **E)** Quantification of

762 Ngfr+ cells was shown in the graphs as a percentage of Itga7+Sca1-Ln- population (n=8 CTR, n=10

763 DEN, Values represent mean ± s.d. ***$P < 0.001$; by Mann-Whitney test).

764

765

A

Nerve Ngfr+

Muscle Ngfr+

RNA-seq

B

PC2: 3% variance

PC1: 94% variance

group
- muNGFR
- neNGFR

C

Row Z-Score
-1 0 1

Pamr1
Tnfrsf23
C1qtnf1
Basp1
Adamts14
P2rx7
Fkbp10
Flt1
Sytl2
Cd36
Cnksr2
Bcor
Cnksr3
Ecm2
Cldn1
Frzb
Matn2
Atf3
Lama4
Sep.11
Aqp1
Sox10
Mical3
Aspa
Dclk1
Smc4
Dbn1
Cthrc1
AI414108
Slitrk6
Tmem88b
Mtss1
Cpxm2
Cdk5r1
Clic5
Nebl
Bmf
Tspan13
Rasgrp3
Cdh23
Slfn4
Hmgcs2
Plac8
Tnc

muNGFR   neNGFR

D

Tnc

Fold to muNGFR

muNGFR   neNGFR

***

Gdnf

Fold to muNGFR

muNGFR   neNGFR

*

Shh

Fold to muNGFR

muNGFR   neNGFR

**

E

Tnc   Btx   Tnc Btx Cav3 Dapi

CTR

DEN

F

Tnc+/Btx+ (%)

CTR   DEN

***

766

35

767

Figure 4. A specific transcriptional signature distinguishes glial cells in muscle from those residing in the nerve

A) Experimental setting for RNA-sequencing analysis of Ngfr+ cells derived from denervated muscle and nerve at 3-days post nerve lesion. **B)** Sample distance - represented as Principal component analysis (PCA) - of transcriptome of Ngfr+ cells derived from denervated muscle and nerve at 3-days post nerve lesion (n=3). **C)** Heatmap representation of genes significantly deregulated - p adj<0.001 – in freshly isolated Ngfr+ cells derived from denervated muscle and nerve at 3-days post nerve lesion (n=3). **D)** qPCR analysis for the expression of Tnc, Gdnf and Shh in freshly isolated Ngfr+ cells derived from denervated muscle (muNGFR) and nerve (neNGFR) at 3-days post nerve lesion (n=4, Values represent mean ± s.d. .*P < 0.05, **P < 0.01 and ***P < 0.001; by student t-test (Tnc, Gdnf) or by Mann-Whitney (Shh)). **E)** Representative immunofluorescence analysis of TA muscle cryosection derived from control and denervated muscle, stained for Tnc (green), Bungarotoxin (Btx, red) and Caveolin-3 (Cav3, Cyan). Arrows highlight Tnc and asterisk highlight Btx. Nuclei were counterstained with dapi. Scale bar = 20μm. **F)** Quantification Bungarotoxin (Btx) and Tnc co-localization in control and denervated muscle (n=3, Values represent mean ± s.d. ***P < 0.001; by student t-test)

784
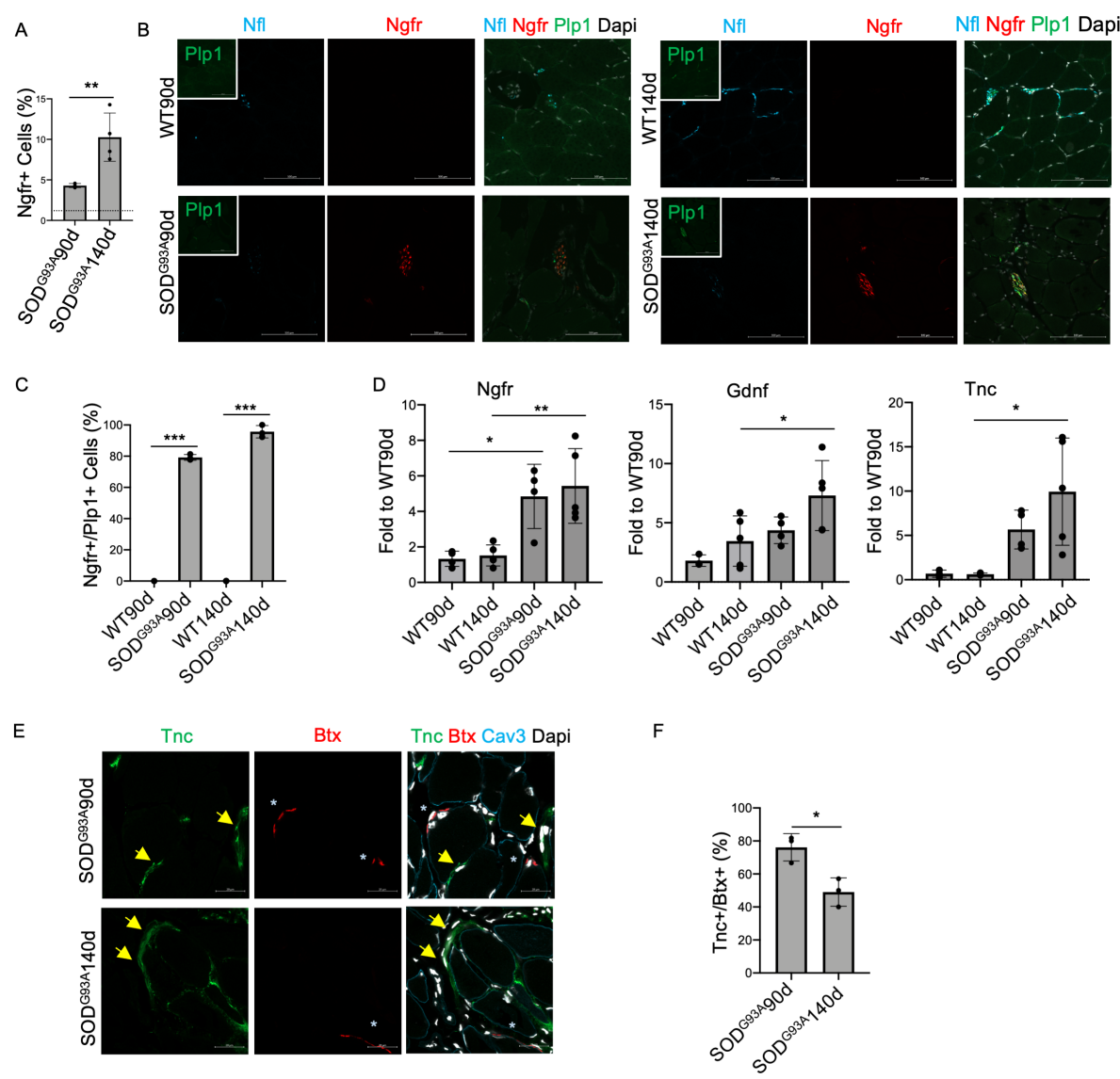
787 **Figure 5. Muscle resident glial cell activation in a mouse model of ALS.**

788 **A)** Ngfr+ cell cytofluorimetric quantification was shown in the graphs as a percentage of Itga7+Sca1-

789 Ln- population, in 90- and 140-days old SOD^{G93A} mice muscle (n=4, Values represent mean ± s.d.

790 **P < 0.01; by One Way Anova Tukey's Multiple Comparisons test). Dotted line highlight percentage

791 in WT mice muscle. **B)** Representative immunofluorescence analysis of TA muscle cryosection

792 derived from 90- and 140-days old SOD^{G93A} and WT mice stained for Neurofilament-L (Nfl, Cyan),

793 Ngfr (red) and Plp1 (green). Nuclei were counterstained with dapi. Scale bar = 100μm. **C)**

794 Quantification graph of Ngfr+/Plp1+ cells in 90- and 140-days old WT and SOD^{G93A} mice muscle

795 (n=3, Values represent mean ± s.d. ***P < 0.001; by One Way Anova Tukey's Multiple Comparisons

796 test) **D)** qPCR analysis for the expression of Ngfr, Gdnf and Tnc in freshly isolated Itga7+Sca1-Ln-

797 cells derived from WT and SOD^{G93A} muscle at 90- and 140-days of post-natal life. Gapdh was used

798 as housekeeping gene (n=4, Values represent mean ± s.d. *P < 0.05 and **P < 0.01; by One Way

799 Anova Tukey's Multiple Comparisons test). **E)** Representative immunofluorescence analysis of TA

800 muscle cryosection derived from 90- and 140-days old SOD^{G93A} and WT mice stained for Tnc

801 (green), Bungarotoxin (Btx, red) and Caveolin-3 (Cav3, Cyan). Arrows highlight Tnc and asterisk

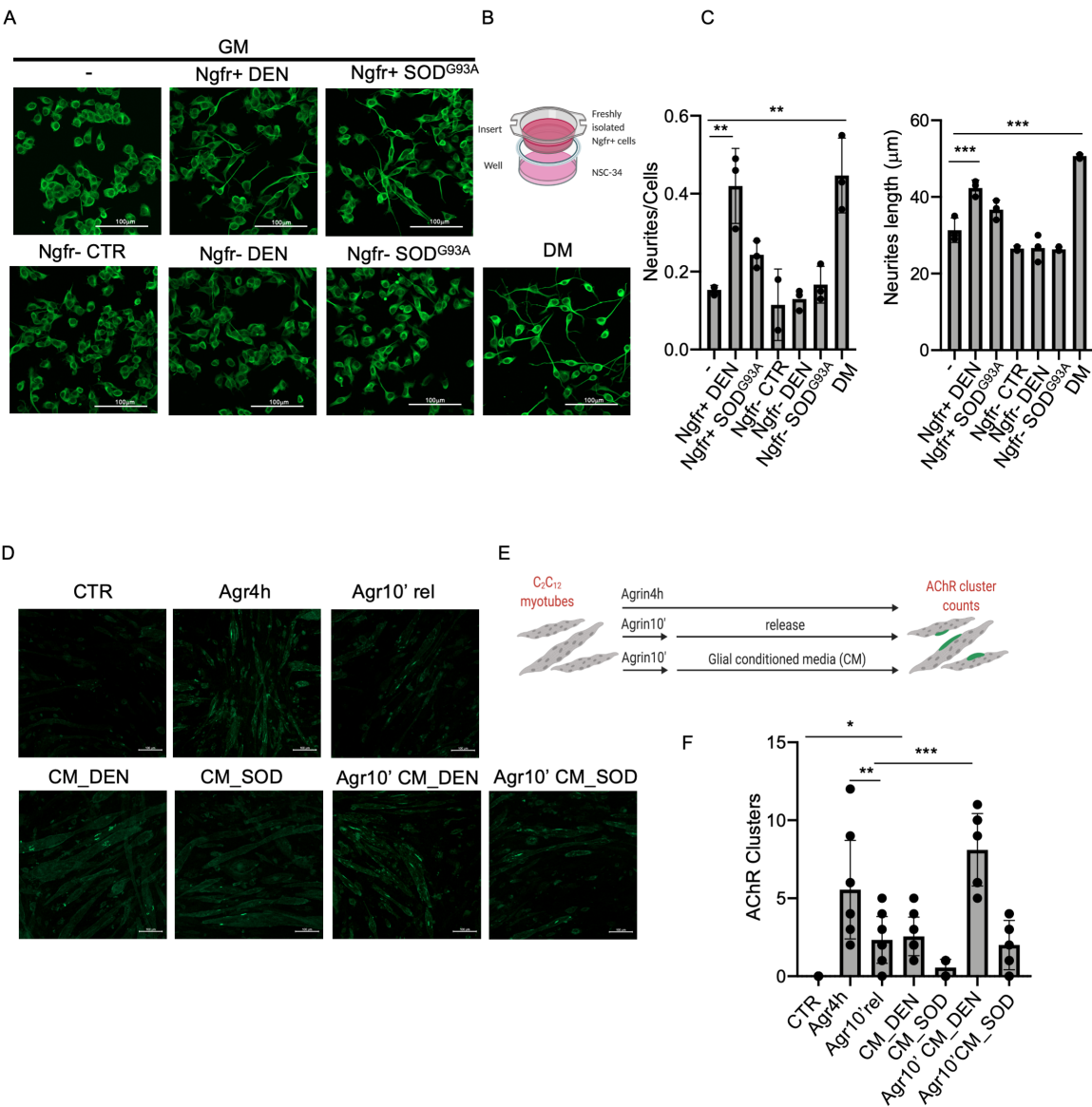802 highlight Btx. Nuclei were counterstained with dapi. Scale bar = 20μm. **F)** Quantification of

803 Bungarotoxin (Btx) and Tnc co-localization in 90- and 140-days old SOD^{G93A} mice muscle (n=3,

804 Values represent mean ± s.d. *P < 0.05; by student t-test)

805

808 **Figure 6. Muscle resident glial cells promote neurite outgrowth and AChR clustering.**

809 **A)** Representative immunofluorescence analysis of NSC-34 cells in growth media cultured either

810 alone (-) or in co-culture with Ngfr+ or with Ngfr- cells, both from denervated muscle and SOD^{G93A}

811 muscle at 90-days of post-natal life, and of NSC-34 cells cultured in neurogenic differentiation media

812 (DM), stained for beta-3-Tubulin (green). Scale bar = 100μm. **B)** Schematic representation of in-vitro

813 co-culture system. **C)** Quantification of neurites number per cell and length of NSC-34 cultured in

814 the indicated conditions (n=3, Values represent mean ± s.d. **$P < 0.01$ and, **$P < 0.01$; by One Way

815 Anova Tukey's Multiple Comparisons test). **D)** Representative immunofluorescence analysis of

816 C2C12 myotubes treated or not with Agrin or conditioned media from glial cells as indicated and

817 stained with Bungarotoxin (Btx, green). Scale bar = 100μm. **E)** Schematic representation of the

818 experimental setting. **F)** Quantification of AChR clustering ($\geq$ 25 μm) (n=5, Values represent mean ±

819 s.d.. *$P < 0.05$, **$P < 0.01$, ***$P < 0.001$; by One Way Anova Tukey's Multiple Comparisons test).

820